Arabian Journal of Chemistry (2022) **15**, 104072

King Saud University

Arabian Journal of Chemistry

www.ksu.edu.sa
www.sciencedirect.com

ORIGINAL ARTICLE

Synthesis and biological evaluation of coumarin derivatives containing oxime ester as α-glucosidase inhibitors

Xin Zhang [a], Ying-Ying Zheng [a], Chun-Mei Hu [a], Xiao-Zheng Wu [a], Jing Lin [a], Zhuang Xiong [a], Kun Zhang [a], Xue-Tao Xu [a,b,*]

[a] *School of Biotechnology and Health Sciences, Wuyi University, Jiangmen 529020, PR China*
[b] *School of Chemistry and Chemical Engineering, Henan Normal University, Xinxiang 453007, PR China*

Received 30 March 2022; accepted 21 June 2022
Available online 26 June 2022

KEYWORDS

Coumarin derivatives;
a-Glucosidase;
Inhibition mechanism;
Molecular docking

Abstract In this study, potent coumarin derivatives containing oxime ester **1** ~ **28** as α-glucosidase inhibitors were developed through a stepwise structure optimization, and the structure activity relationship was uncovered. Among them, compound **20** exhibited outstanding α-glucosidase inhibitory activity with IC_{50} of 2.54 ± 0.04 μM compared to 640.57 ± 1.13 μM of Acarbose. Kinetic study ascertained that compound **20** was a reversible and uncompetitive α-glucosidase inhibitor. 3D fluorescence results showed that the interaction of compound **20** with α-glucosidase caused the changes of microenvironments and polypeptide backbone structure of α-glucosidase. CD spectra results revealed that compound **20** decreased the α-helix content and increased the β-sheet content. Molecular docking analysis indicated that compound **20** well located into the active site and mainly bind with Phe157, His239, His279, Tyr71, and Arg312 to reduce the catalytic activity of α-glucosidase.

1. Introduction

Type 2 diabetes mellitus (T2DM) is a metabolic disease characterized by hyperglycemia resulting from insulin resistance and insufficient insulin secretion by pancreatic β-cells. One of key reasons for the hyperglycemia is the enzymatic hydrolysis of carbohydrates. α-Glucosidase (EC 3.2.1.20), an *exo*-acting carbohydrase, locate in the human small intestine (Proença et al., 2017). It catalyzes hydrolysis of carbohydrate substrates to release α-D-glucopyranose (Ali et al., 2017). Excessive absorbed glucopyranose leads to the abnormal increase of blood glucose concentration, and long-term high blood glucose accelerates the non-enzymatic glycosylation to produce a large amount of advanced glycation end products (AGEs), thereby causing

* Corresponding author at: School of Biotechnology and Health Sciences, Wuyi University, Jiangmen 529020, PR China.
E-mail address: wyuchemxxt@126.com (X.-T. Xu).
Peer review under responsibility of King Saud University.

Production and hosting by Elsevier

https://doi.org/10.1016/j.arabjc.2022.104072
1878-5352

a series of complications of diabetes (Tsoutsouki et al., 2020). The inhibition of α-glucosidase activity leads to the retardation of carbohydrates digestion, and thereby resulting in the reduction of glucose absorption (Imran et al., 2015). The action mechanism of α-glucosidase inhibitors is attributed to their competitive binding to the carbohydrate-binding region of α-glucosidase (Sohretoglu et al., 2018). α-Glucosidase inhibitors have been reported to be used as effective agents in the treatment of carbohydrate metabolism related diseases, including diabetes, HIV, obesity, and dyslipidemia (Rasouli et al., 2017; Santos et al., 2018). Currently, some α-glucosidase inhibitor drugs have been used in the clinic, such as acarbose, voglibose, and miglitol. However, the clinical application found that those drugs still have some adverse side effects, which also limit their clinical use (Hedrington and Davis, 2019). Thence, it is urgent to develop more effective and lower toxic α-glucosidase inhibitors.

Coumarin, 2-γ-benzopyrones, is a vital core skeleton present in a large amount of natural and synthetic compounds (Stefanachi et al., 2018). Compounds containing coumarin moiety had been revealed to display various pharmacological activities, including anti-inflammatory, anti-bacterial, antiviral, anti-oxidation, anti-cancer (Wu et al., 2020; Matos et al., 2017; Sahni et al., 2021). In particularly, lots of natural and synthetic compounds containing coumarin moiety presented potential α-glucosidase inhibitory activity and hypoglycemic activity (Wang et al., 2016; Salar et al., 2016; Taha et al., 2018). Our previous study also demonstrated that coumarin moiety could act as the important core skeleton in designed α-glucosidase inhibitors (Xu et al., 2020). Some of the representative α-glucosidase inhibitors containing coumarin moiety were shown in Fig. 1. On the other hand, oxime ester serviced as an important active skeleton in many drugs, and showed many biological activities, such as bactericidal, anti-inflammatory and antiviral (Kassa et al., 2017; Schepetkin et al., 2021). Also, some oxime ester derivatives showed potent α-glucosidase inhibitory and hypoglycemic activity (Fig. 1) (Hosseini Ghazvini et al., 2018; Tran et al., 2022). Furthermore, benzoic acid and cinnamic acid also play important roles in many α-glucosidase inhibitors or hypoglycemic drugs (Fig. 1) (Hameed et al., 2019; Song et al., 2016).

According to the findings above, the hybridization of coumarin with cinnamic acid and benzoic acid through oxime linkage was developed aiming to obtain new α-glucosidase inhibitors (Fig. 2, design strategy). All synthesized compounds were assayed for their α-glucosidase.

2. Results and discussion

2.1. Chemistry

The target coumarin derivatives **1** ~ **28** were synthesized according to the synthetic route illustrated in Schemes 1. Substituted salicylaldehyde underwent perkins reaction with ethyl acetaacetate to obtain substituted acetyl coumarin, which reacted with hydroxylamine hydrochloride to produce coumarin containing oxime. Finally, target coumarin derivatives **1** ~ **28** were obtained from the esterification of coumarin containing oxime with substituted benzoic acid or substituted cinnamic acid. All coumarin derivatives **1** ~ **28** were identified by ^{1}H NMR, ^{13}C NMR and HRMS.

2.2. α-Glucosidase inhibition assay and structure–activity relationships (SAR) analysis

At the beginning, to develop more potent α-glucosidase inhibitors and ascertain the SAR, compounds **1** ~ **9** (containing benzoyl) and compounds **10** ~ **18** (containing cinnamic acyl) were preferable synthesized through the scaffold hybridization strategy. Then the synthesized coumarin derivatives were assayed for their *in vitro* α-glucosidase inhibitory activity with commercially α-glucosidase inhibitor acarbose as a positive control. The results showed that coumarin derivatives **1** ~ **18** demonstrated excellent and potent inhibitory activity against α-glucosidase with the IC_{50} range of 5.06 ± 0.08 ~ 93.23 ± 0.25 μM, as compared to the standard acarbose (IC_{50} = 640.57 ± 1.13 μM) (Table 1). These results showed that the hybridization of coumarin with substituted cinnamic acid or benzoic acid through oxime linkage could obtain potential α-glucosidase inhibitors.

Then the SAR was analyzed based on activity data. For compounds **1** ~ **9** (containing benzoyl), compound **1** without substituent group presented an IC_{50} of 93.23 ± 0.25 μM. Compounds **2** ~ **9** with different substituent group showed stronger inhibitory activity than compound **1**, suggesting the introduction of substituent group (as shown by CH_3, Cl, Br, F, OCH_3, NO_2, CF_3, or OH) could effectively enhance the inhibitory activity. Among them, Bromine substituent (Br) showed the strongest enhancement on the inhibitory activity. Similar for compounds **10** ~ **18** (containing cinnamic acyl), it was also observed that compounds **11** ~ **18** with substituent group (CH_3, Cl, Br, F, OCH_3, NO_2, CF_3, or OH) at benzene ring of cinnamic acid displayed stronger inhibitory activity than compound **10** (without substituent group), revealing that the introduction of substituent group was vital for the α-glucosidase inhibition. Furthermore, compounds **10** ~ **18** (containing cinnamic acyl) showed higher α-glucosidase inhibi-

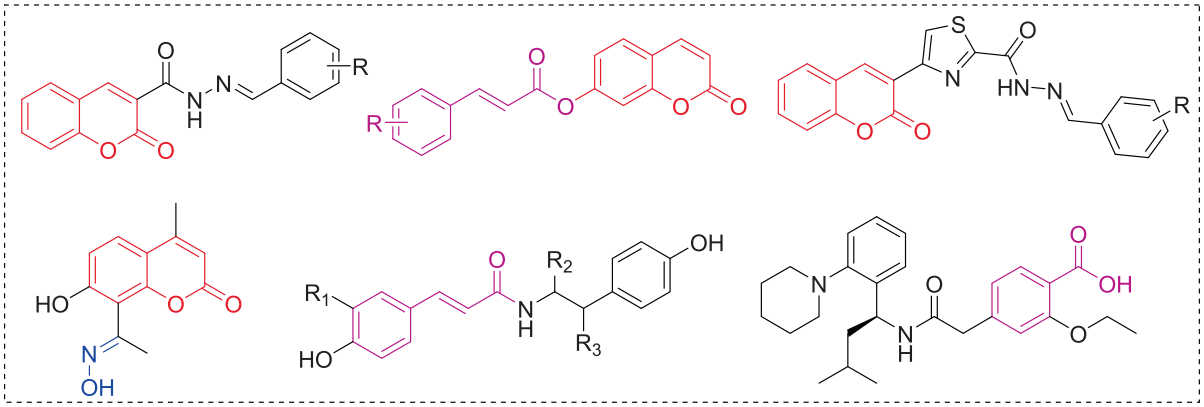

Fig. 1 Chemical structures of some reported α-glucosidase inhibitors containing coumarin (Red color), oxime ester (Blue color), and benzoyl or cinnamic acyl moiety (Pink color).

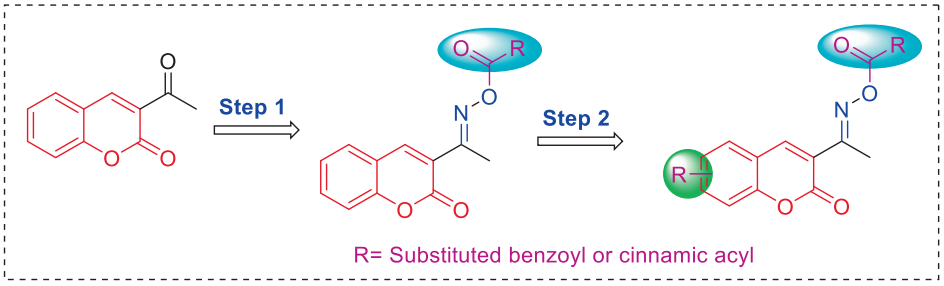

Fig. 2 Design strategy of target coumarin compounds.

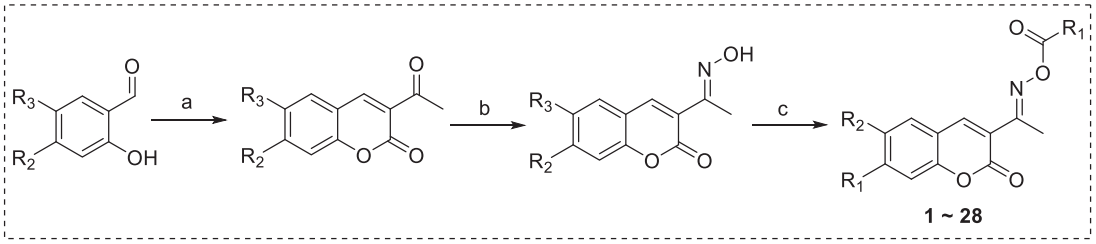

Scheme 1 Synthesis of coumarin derivatives **1** ~ **28**. Reagents and condition: (a) Ethyl Acetaacetate, Pi3peridine, EtOH; (b) Hydroxylamine hydrochloride, Pyridine, EtOH; (c) Substituted benzoic acid chloride or substituted cinnamic acid chloride, triethylamine, DCM.

tory activity than compounds **1** ~ **9** (containing benzoyl) with the same substituent group, respectively, suggesting that cinnamic acyl was more beneficial for α-glucosidase inhibition than benzoyl. Among them, compound **13** (containing bromcinnamic acyl) showed the highest inhibitory activity (IC_{50} = 5.06 ± 0.08 μM).

Then, coumarin fragment of the compound was further optimized based on compound **13**, subsequently producing compounds **19** ~ **28**. Their α-glucosidase inhibition results showed that the introduction of substituent group (Cl, Br, or F) at **C-6** or **C-7** position of coumarin could efficiently increase the inhibitory activity. However, substituent group (CH_3, or OCH_3) was introduced at **C-6** or **C-7** position of coumarin, leading to a negative effect. In particularly, compound **20** containing Br at **C-7** position of coumarin fragment showed the best α-glucosidase inhibitory activity with an IC_{50} of 2.54 ± 0.04 μM. The physicochemical properties of 3f were predicted and shown in Table 2.

From aforementioned results, it could easily be extracted that the α-glucosidase inhibitory activity of coumarin derivatives **1** ~ **28** was depending upon the characteristic of oxime ester (benzoyl or cinnamic acyl) and substituent group on benzoyl, cinnamic acyl or coumarin.

2.3. Inhibitory mechanism and type assay

To analyze the action mechanisms of α-glucosidase inhibition of all coumarin derivatives, enzyme kinetic analysis was performed on the most potent compound **20**. As illustrated in Fig. 3a, the plots of residual enzyme activity *versus* enzyme concentration in the presence of compound **20** (0 ~ 4 μM) gave a family of straight lines with common intersection at the origin, indicating that compound **20** is a reversible inhibitor (Ali et al., 2017).

The kinetic type of compound **20** on α-glucosidase inhibition was also performed using Lineweaver-Burk plots of residual enzyme activity *versus* substrate concentration (Fig. 3b). As revealed from the Lineweaver-Burk plots, the data lines of compound **20** intersected in the x axis thereby indicating a noncompetitive inhibition (Tsoutsouki et al., 2020). Moreover, thire slop *versus* inhibitor concentrations of compound **20** to produce the inhibition constant (K_I) was calculated as 1.5 μM.

2.4. Three-dimensional (3D) fluorescence spectra assay

The 3D fluorescence spectra was used to analyze the conformational changes of α-glucosidase interacting with compound **20**. In the three-dimensional fluorescence spectrum of α-glucosidase alone (Fig. 4a), Peak **1** (λ_{ex} = 276 nm, λ_{em} = 330 - nm) reflected the fluorescence spectra of Tyr with Trp residues, and Peak **2** (λ_{ex} = 232 nm, λ_{em} = 332 nm) denoted the fluorescence feature of polypeptide backbone structure. After treated with compound **20** (concentration 2 μM), the fluorescence intensity of Peak **1** reduced by 13.45%, and Peak **2** decreased by 37.04% (Fig. 4b), suggesting that the interaction of compound **20** with α-glucosidase caused the changes of microenvironments of the tyrosine and tryptophan residues and the polypeptide backbone structure of α-glucosidase.

2.5. CD spectra assay

The conformational changes, especially the secondary structures changes, of α-glucosidase was monitored by the CD spectra. As shown in Fig. 5, two negative bands appeared at 210 and 222 nm, which were defined as the typical features of α-helixes. While treatment of compound **20** lead to the obviously reduce of negative bands intensity (Table 3). Treatment of

Table 1 The α-glucosidase inhibitory activity assay of coumarin derivatives **1** ∼ **28**.

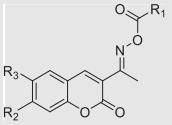

Compound	R_1	R_2	R_3	α-glucosidase inhibition (IC_{50} μM)
1		H	H	93.23 ± 0.25#
2		H	H	15.91 ± 0.25#
3		H	H	10.95 ± 0.11#
4	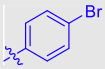	H	H	6.46 ± 0.05#
5		H	H	29.21 ± 0.32#
6	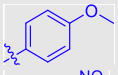	H	H	19.34 ± 0.22#
7	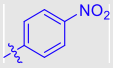	H	H	26.12 ± 0.26#
8	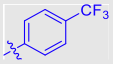	H	H	26.16 ± 0.26#
9	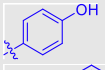	H	H	26.14 ± 0.26#
10	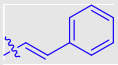	H	H	34.35 ± 0.31#
11	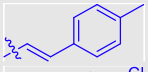	H	H	13.39 ± 0.09#
12	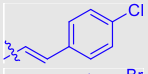	H	H	6.34 ± 0.05#
13	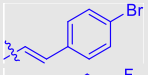	H	H	5.06 ± 0.08#
14	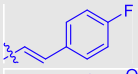	H	H	11.55 ± 0.13#
15	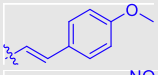	H	H	15.09 ± 0.10#
16	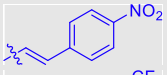	H	H	8.71 ± 0.21#
17	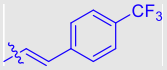	H	H	19.66 ± 0.04#
18	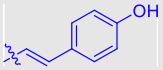	H	H	21.54 ± 0.02#
19	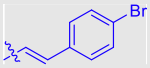	Cl	H	3.42 ± 0.07#
20	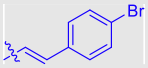	Br	H	2.54 ± 0.04#
21	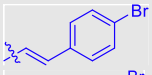	F	H	3.92 ± 0.02#
22	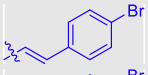	CH_3	H	5.24 ± 0.16#
23	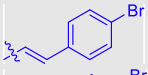	OCH_3	H	6.43 ± 0.06#
24	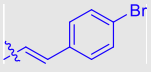	H	Cl	4.25 ± 0.02#

Table 1 (*continued*)

Compound	R_1	R_2	R_3	α-glucosidase inhibition (IC_{50} μM)
25	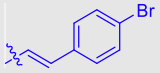	H	Br	3.81 ± 0.14#
26	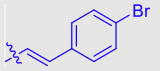	H	F	3.73 ± 0.10#
27	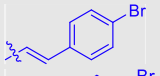	H	CH_3	6.17 ± 0.04#
28	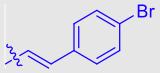	H	OCH_3	7.84 ± 0.14#
Acarbose				640.57 ± 1.13

Values are shown in mean ± SD. #Indicating comparisons between the compound and acarbose (#P < 0.05).

Table 2 The physicochemical properties of compound **20**.

	Molecular formula	Molecular weight	Rotatable bonds	H-bond acceptoer atoms	H-bond donnor atoms	Polar surface area (Å2)	LogPo/w	Water solubility
compound **20**	$C_{20}H_{13}Br_2NO_4$	491.13	5	5	0	68.87	5.01	Poorly soluble

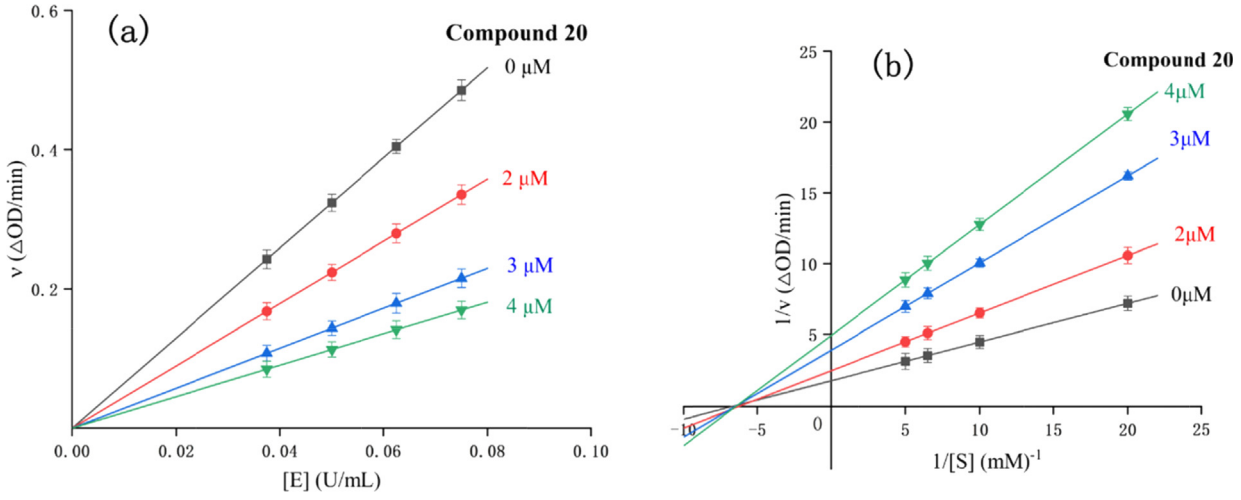

Fig. 3 Inhibitory mechanism (a) and type assay (b) of compound **20** against α-glucosidase.

compound **20** (molar ratios: 3:1) caused a decrease in the content of the α-helix (from 10.40 to 9.40%), β-turn (from 20.10 to 19.40%), and random coil (from 33.20 to 32.00%), while an increase in antiparallel (from 35.10 to 39.30%), respectively. These results revealed that compound **20** bound to α-glucosidase and rearranged its secondary structure.

2.6. Molecular docking

Molecular docking was performed to analyze the binding mode of compound **20** to α-glucosidase. The docking results between compound **20** and α-glucosidase was shown in Fig. 6. Compound **20** well located into the active site with a "U shaped" conformation, and cinnamic acid part nested inside of the active site (Fig. 6a∼c). The detailed interaction results were shown out using 3D view (Fig. 6c) and 2D view (Fig. 6d), respectively. It was observed that the carbonyl of coumarin and nitrogen of oxime formed hydrogen bonds with Arg312, respectively (bond length: 1.9 Å and 2.4 Å), which was recognized as the key interaction between compound **20** and α-glucosidase. The bromcoumarin fragment formed Pi-Pi stacking with Phe157 (4.4 Å) and Pi-Alkyl interactions His239 and His279. Moreover, the bromcinnamic acyl formed Pi-Alkyl interactions with Tyr71. All above interactions helped compound **20** to anchor in the active site of the α-glucosidase.

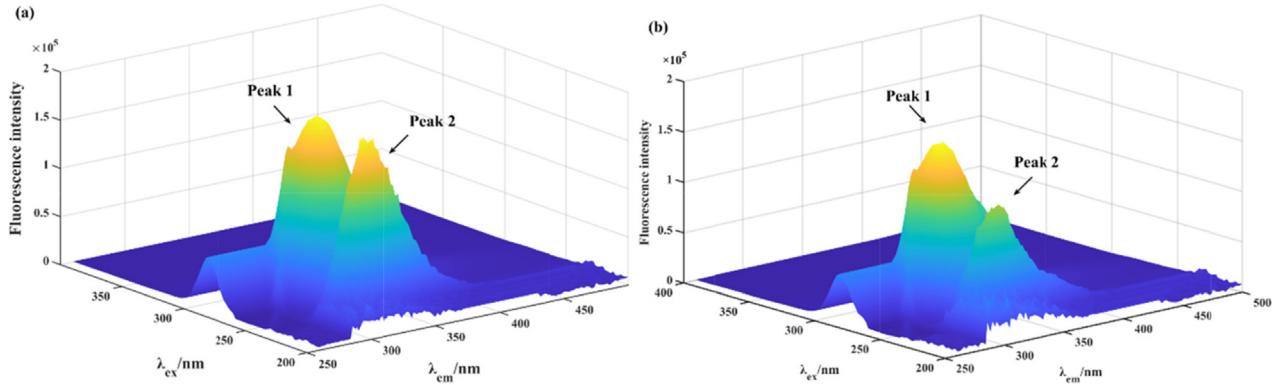

Fig. 4 The 3D fluorescence spectra of α-glucosidase (a) and α-glucosidase with compound **20** system (b).

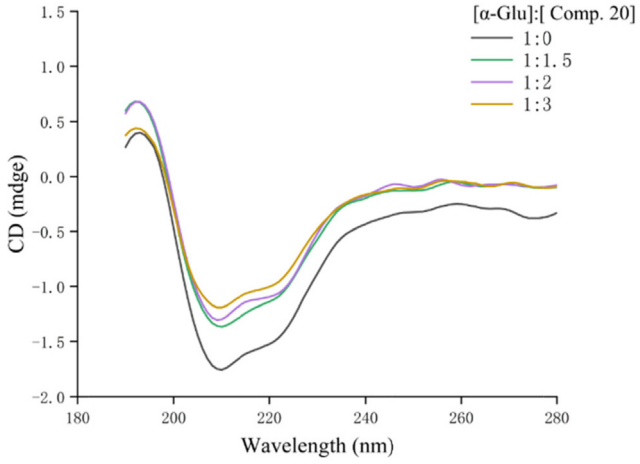

Fig. 5 CD spectra of α-glucosidase in the presence of compound **20**.

Table 3 The secondary structures contents of α-glucosidase with compound **20** complex.

Molar ratio [α-Glu]:[Comp.20]	α-Helix (%)	β-Sheet (%)	β-Turn (%)	Rndm Coil (%)
1:0	10.40	35.10	20.10	33.20
1:1.5	10.00	39.00	19.50	31.80
1:2	9.90	39.20	19.50	31.80
1:3	9.40	39.30	19.40	32.00

3. Conclusion

In summary, coumarin derivatives containing oxime ester **1** ~ **28** were s ynthesized and evaluated for inhibitory activities against α-glucosidase. All the synthesized coumarin derivatives showed potent inhibitory activities against α-glucosidase and stronger than acarbose. The inhibition kinetic studies, CD spectra, 3D fluorescence, and docking simulation indicated the binding between compound **20** with α-glucosidase. Considering all these experimental data, coumarin derivatives containing oxime ester might be used as leading compound to find effective drugs for the management of T2D.

4. Experimental

4.1. Materials and methods

α-Glucosidase from *Saccharomyces cerevisiae* (EC 3.2.1.20) was purchased from Sigma-Aldrich. *p*-Nitrophenyl-α-D-galactopyranoside (PNPG) was obtained from Abcam. All other reagents and solvents were commercial available. ^{1}H NMR and ^{13}C NMR spectra were recorded in $CDCl_3$ on 500 MHz instruments. High-resolution mass spectral analysis (HRMS) data were measured on the Apex II by means of the ESI technique.

*4.2. General procedure for the synthesis of coumarin derivatives **1** ~ **28***

A mixture of substituted salicylaldehyde (1.0 mmol), ethyl acetoacetate (1.1 mmol), and piperidine (0.02 mmol) in ethanol (10 mL) was stirred at 70 °C for 2 h. After the reaction was completed, the mixture was poured into ice-cold water, followed by the filtration to obtain the crude product. Then the substituted acetyl coumarin was yield by recrystallization from ethanol.

The mixture of substituted acetyl coumarin (1.0 mmol), hydroxylamine hydrochloride (3.0 mmol), and pyridine (0.04 mmol) in ethanol (10 mL) was stirred at room temperature for 20 h. The produced solid was filtered and washed with ethanol to produce substituted acetyl coumarin containing oxime.

To the ice bath solution of substituted acetyl coumarin containing oxime (1.0 mmol) and triethylamine (1.1 mmol) in DCM (3 mL), the substituted benzoic acid chloride or substituted cinnamic acid chloride in DCM (3 mL) was added, and then reacted for 12 h after warming to room temperature. After quenched by water, the mixture was extracted with dichloride for three times, and washed with brine, dried by $MgSO_4$. The solvent was removed under vacuum to obtain the crude product, followed by purification through column chromatography to yield the corresponding coumarin derivatives **1** ~ **28**.

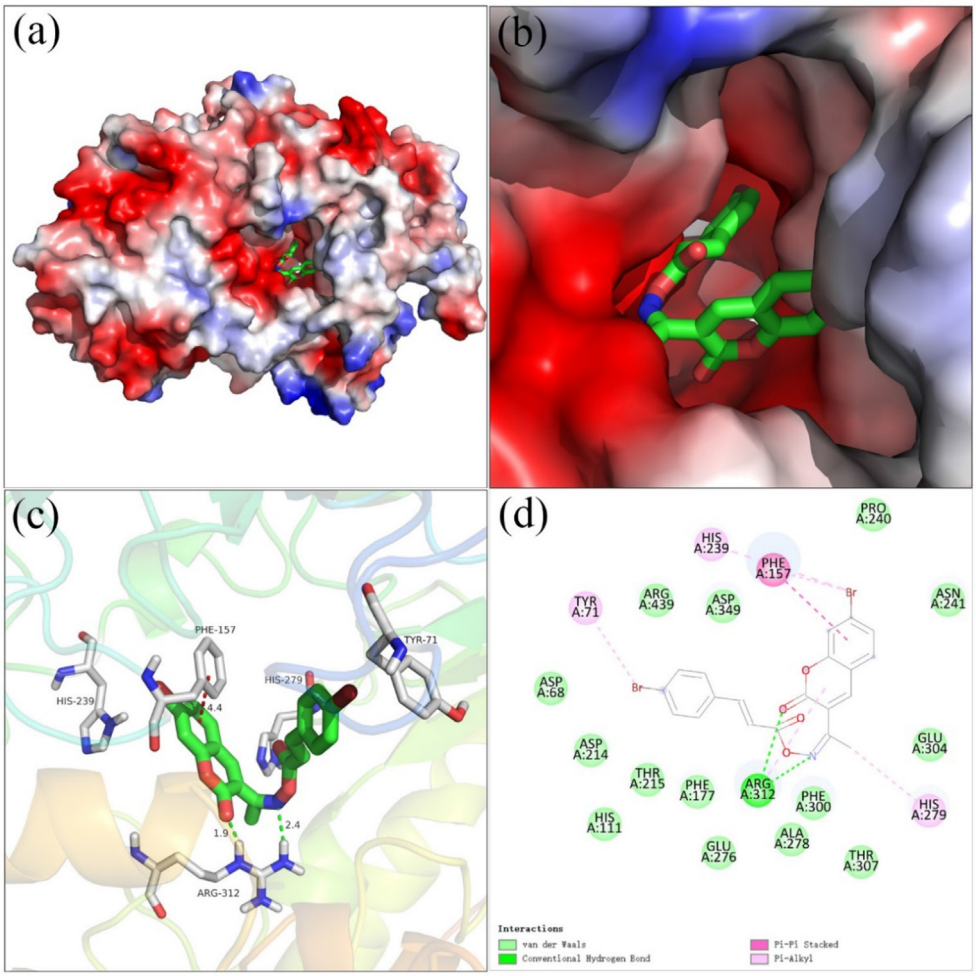

Fig. 6 The molecular docking of compound **20** and α-glucosidase, (a, b) compound **20** in the electrostatics active pocket, (c) 3D view of compound **20** with α-glucosidase, (d) 2D view of compound **20** with α-glucosidase.

(1, $C_{18}H_{13}NO_4$). White sold; Yield 72%; m.p. 157–159 °C; ^{1}H NMR (500 MHz, Chloroform-*d*) δ 8.20 (s, 1H), 8.13 (dd, *J* = 8.1, 1.5 Hz, 2H), 7.66–7.57 (m, 3H), 7.51 (t, *J* = 7.7 Hz, 2H), 7.39–7.30 (m, 2H), 2.55 (s, 3H); ^{13}C NMR (126 MHz, $CDCl_3$) δ 163.60, 162.71, 159.25, 154.37, 143.51, 133.67, 133.02, 129.76, 129.09, 128.71, 128.66, 124.98, 123.48, 118.53, 116.70, 77.33, 77.07, 76.82, 16.03; HRMS (ESI) $[M + H]^+$ calcd. for $C_{18}H_{13}NO_4$:308.0914; found: 308.0926.

(2, $C_{19}H_{15}NO_4$). White sold; Yield 70%; m.p. 160–161 °C; ^{1}H NMR (500 MHz, Chloroform-*d*) δ 8.20 (s, 1H), 8.02 (d, *J* = 8.0 Hz, 2H), 7.59 (t, *J* = 7.6 Hz, 2H), 7.37 (d, *J* = 8.3 Hz, 1H), 7.35–7.28 (m, 3H), 2.55 (s, 3H), 2.44 (s, 3H); ^{13}C NMR (126 MHz, $CDCl_3$) δ 163.76, 162.54, 159.21, 154.35, 144.86, 143.46, 133.06, 129.07, 128.47, 126.00, 125.97, 124.99, 123.42, 118.49, 117.96, 116.70, 77.32, 77.07, 76.81, 15.97; HRMS (ESI) $[M + H]^+$ calcd. for $C_{19}H_{15}NO_4$: 322.1071; found:322.1084.

(3, $C_{18}H_{12}ClNO_4$). White sold; Yield 70%; m.p. 185–186 °C; ^{1}H NMR (500 MHz, Chloroform-*d*) δ 8.19 (s, 1H), 8.06 (dd, *J* = 8.5, 1.6 Hz, 2H), 7.61–7.57 (m, 2H), 7.49 (dd, *J* = 8.4, 1.6 Hz, 2H), 7.39–7.31 (m, 2H), 2.55 (d, *J* = 1.5 Hz, 3H); ^{13}C NMR (126 MHz, $CDCl_3$) δ 162.98, 162.81, 159.23, 154.38, 143.59, 140.23, 133.12, 131.13, 129.12, 127.07, 125.02, 123.33, 118.48, 116.74, 77.31, 77.26, 77.05, 76.80, 16.09; HRMS (ESI) $[M + H]^+$ calcd. for $C_{18}H_{12}ClNO_4$: 342.0525; found: 342.0536.

(4, $C_{18}H_{12}BrNO_4$). White sold; Yield 69%; m.p. 180–182 °C; ^{1}H NMR (500 MHz, Chloroform-*d*) δ 8.18 (s, 1H), 8.00–7.97 (m, 2H), 7.66–7.64 (m, 2H), 7.62–7.57 (m, 2H), 7.38–7.31 (m, 2H), 2.54 (s, 3H); ^{13}C NMR (126 MHz, $CDCl_3$) δ 163.01, 162.94, 159.20, 154.38, 143.58, 133.12, 132.11, 131.22, 129.11, 128.91, 127.53, 125.02, 123.31, 118.48, 116.73, 77.32, 77.07, 76.81, 16.08; HRMS (ESI) $[M + H]^+$ calcd. for $C_{18}H_{12}BrNO_4$: 387.9997; found: 388.0004.

(5, $C_{18}H_{12}FNO_4$). White sold; Yield 68%; m.p. 208–209 °C; ^{1}H NMR (500 MHz, Chloroform-*d*) δ 8.19 (s, 1H), 8.17–8.14 (m, 2H), 7.61–7.58 (m, 2H), 7.39–7.31 (m, 2H), 7.19 (t, *J* = 8.6 Hz, 2H), 2.55 (s, 3H); ^{13}C NMR (126 MHz, $CDCl_3$) δ 167.17, 165.13, 162.82, 162.67, 159.23, 154.39, 143.54, 133.08, 132.41, 132.33, 129.10, 125.00, 124.89, 124.86, 123.38, 118.51, 116.73, 116.08, 115.90, 77.30, 77.25, 77.04, 76.79, 16.04; HRMS (ESI) $[M + H]^+$ calcd. for $C_{18}H_{12}FNO_4$: 326.0820; found: 326.0832.

(6, $C_{19}H_{15}NO_5$). White sold; Yield 65%; m.p. 165–167 °C; ^{1}H NMR (500 MHz, Chloroform-*d*) δ 8.20 (s, 1H), 8.10 – 8.08 (m, 2H), 7.59 (d, *J* = 7.7 Hz, 2H), 7.39–7.31 (m, 2H), 7.00–6.97 (m, 2H), 3.90 (s, 3H), 2.54 (s, 3H); ^{13}C NMR (126 MHz, $CDCl_3$) δ 163.93, 163.38, 162.21, 159.33, 154.36,

143.45, 132.97, 131.90, 129.08, 124.97, 123.60, 120.79, 118.57, 116.70, 114.00, 77.30, 77.25, 77.05, 76.79, 55.56, 16.00; HRMS (ESI) $[M + H]^+$ calcd. for $C_{19}H_{15}NO_5$: 338.1019; found: 338.1033.

(7, $C_{18}H_{12}N_2O_6$). Yellow sold; Yield 65%; m.p. 244–245 °C; ^{1}H NMR (500 MHz, Chloroform-*d*) δ 8.38 – 8.36 (m, 2H), 8.32 – 8.29 (m, 2H), 8.19 (s, 1H), 7.64–7.59 (m, 2H), 7.40–7.33 (m, 2H), 2.58 (s, 3H); ^{13}C NMR (126 MHz, $CDCl_3$) δ 163.82, 161.81, 159.13, 154.43, 150.89, 143.74, 134.15, 133.30, 130.89, 129.16, 127.73, 125.09, 123.89, 123.80, 123.04, 118.40, 116.78, 77.30, 77.25, 77.05, 76.79, 16.20; HRMS (ESI) $[M + H]^+$ calcd. for $C_{19}H_{15}NO_5$: 338.1019; found: 338.1033.

(8, $C_{19}H_{12}F_3NO_4$). White sold; Yield 69%; m.p. 168–170 °C; ^{1}H NMR (500 MHz, DMSO d_6) δ 8.37 (s, 1H), 8.03 – 8.01 (m, 2H), 7.91 (dd, J = 7.8, 1.7 Hz, 1H), 7.83–7.81 (m, 2H), 7.71 (ddd, J = 8.8, 7.4, 1.7 Hz, 1H), 7.51–7.47 (m, 1H), 7.43 (td, J = 7.5, 1.1 Hz, 1H), 2.45 (s, 3H); ^{13}C NMR (126 MHz, DMSO) δ 163.93, 162.59, 159.07, 154.24, 143.92, 133.74, 132.69, 131.84, 130.08, 128.58, 127.85, 125.48, 123.43, 118.83, 116.71, 40.45, 40.38, 40.29, 40.21, 40.12, 40.04, 39.95, 39.87, 39.79, 39.62, 39.45, 16.35; HRMS (ESI) $[M + H]^+$ calcd. for $C_{19}H_{15}NO_4$: 402.0944; found: 402.0951.

(9, $C_{18}H_{13}NO_5$). White sold; Yield 68%; m.p. 159–160 °C; ^{1}H NMR (500 MHz, DMSO d_6) δ 10.53 (s, 1H), 8.36 (s, 1H), 7.98–7.94 (m, 2H), 7.91 (dd, J = 7.8, 1.6 Hz, 1H), 7.74–7.69 (m, 1H), 7.50 (d, J = 8.3 Hz, 1H), 7.43 (t, J = 7.5 Hz, 1H), 6.96–6.90 (m, 2H), 2.43 (s, 3H); ^{13}C NMR (126 MHz, DMSO) δ 163.08, 162.98, 162.77, 159.17, 154.20, 143.71, 133.63, 132.28, 130.02, 125.46, 123.71, 118.94, 118.88, 116.69, 116.18, 40.45, 40.37, 40.28, 40.21, 40.12, 40.04, 39.95, 39.87, 39.78, 39.62, 39.45, 16.22; HRMS (ESI) $[M + H]^+$ calcd. for $C_{18}H_{13}NO_5$: 324.0863; found: 324.08.

(10, $C_{20}H_{15}NO_4$). White sold; Yield 67%; m.p. 161–162 °C; ^{1}H NMR (500 MHz, Chloroform-*d*) δ 8.16 (s, 1H), 7.88 (d, J = 16.0 Hz, 1H), 7.62–7.55 (m, 4H), 7.45–7.38 (m, 3H), 7.38–7.29 (m, 2H), 6.59 (d, J = 16.0 Hz, 1H), 2.49 (s, 3H); ^{13}C NMR (126 MHz, $CDCl_3$) δ 164.32, 162.14, 159.26, 154.34, 146.84, 143.39, 134.14, 132.96, 130.85, 129.06, 129.02, 128.35, 124.95, 123.58, 118.55, 116.68, 115.29, 77.32, 77.06, 76.81, 15.94; HRMS (ESI) $[M + H]^+$ calcd. for $C_{20}H_{15}NO_4$: 334.1070; found: 334.1074.

(11, $C_{21}H_{17}NO_4$). White sold; Yield 62%; m.p. 154–155 °C; ^{1}H NMR (500 MHz, DMSO d_6) δ 8.34 (s, 1H), 7.90 (dd, J = 7.8, 1.6 Hz, 1H), 7.81 (d, J = 16.1 Hz, 1H), 7.69 (dd, J = 7.5, 4.0 Hz, 3H), 7.48 (d, J = 8.3 Hz, 1H), 7.42 (td, J = 7.5, 1.1 Hz, 1H), 7.27 (d, J = 7.8 Hz, 2H), 6.79 (d, J = 16.0 Hz, 1H), 2.38 (s, 3H), 2.34 (s, 3H). ^{13}C NMR (126 MHz, DMSO) δ 164.18, 162.56, 159.13, 154.19, 146.68, 143.72, 141.46, 133.63, 131.70, 130.07, 130.02, 129.14, 125.45, 123.64, 118.87, 116.68, 114.93, 40.48, 40.39, 40.31, 40.23, 40.14, 40.05, 39.98, 39.88, 39.81, 39.64, 39.47, 21.56, 16.15. HRMS (ESI) $[M + H]^+$ calcd. for $C_{21}H_{17}NO_4$: 348.1229; found: 348.1233.

(12, $C_{20}H_{14}ClNO_4$). White sold; Yield 65%; m.p. 248–249 °C; ^{1}H NMR (500 MHz, Chloroform-*d*) δ 8.15 (s, 1H), 7.83 (d, J = 16.0 Hz, 1H), 7.63–7.55 (m, 2H), 7.55–7.49 (m, 2H), 7.41–7.29 (m, 4H), 6.56 (d, J = 16.0 Hz, 1H), 2.48 (s, 3H). ^{13}C NMR (126 MHz, $CDCl_3$) δ 164.09, 162.28, 159.24, 154.32, 145.34, 143.43, 136.78, 133.02, 132.60, 129.52, 129.32, 129.07, 124.98, 123.49, 118.50, 116.69, 115.86, 77.35, 77.09, 76.84, 15.97. HRMS (ESI) $[M + H]^+$ calcd. for $C_{20}H_{14}ClNO_4$: 368.0682, found: 368.0687.

(13, $C_{20}H_{14}BrNO_4$). White sold; Yield 69%; m.p. 182–183 °C; ^{1}H NMR (500 MHz, Chloroform-*d*) δ 8.15 (s, 1H), 7.81 (d, J = 16.0 Hz, 1H), 7.62–7.53 (m, 4H), 7.52 – 7.43 (m, 2H), 7.38–7.30 (m, 2H), 6.58 (d, J = 16.0 Hz, 1H), 2.48 (s, 3H); ^{13}C NMR (126 MHz, $CDCl_3$) δ 164.10, 162.31, 159.26, 154.34, 145.44, 143.45, 133.03, 132.29, 129.71, 129.09, 125.20, 124.99, 123.50, 118.52, 116.71, 115.97, 77.31, 77.26, 77.06, 76.80, 15.98. HRMS (ESI) $[M + H]^+$ calcd. For $C_{20}H_{14}BrNO_4$: 412.0187; found: 412.0181.

(14, $C_{20}H_{14}FNO_4$). White sold; Yield 67%; m.p. 166–170 °C; ^{1}H NMR (500 MHz, Chloroform-*d*) δ 8.14 (s, 1H), 7.84 (d, J = 16.0 Hz, 1H), 7.58 (ddd, J = 9.4, 4.8, 2.3 Hz, 4H), 7.38–7.28 (m, 2H), 7.10 (t, J = 8.6 Hz, 2H), 6.51 (d, J = 16.0 Hz, 1H), 2.48 (s, 3H); ^{13}C NMR (126 MHz, $CDCl_3$) δ 165.21, 164.20, 163.20, 162.18, 159.24, 154.33, 145.47, 143.38, 132.98, 130.43, 130.40, 130.33, 130.26, 129.06, 124.96, 123.55, 118.52, 116.68, 116.30, 116.12, 115.04, 115.02, 77.33, 77.27, 77.07, 76.82, 15.93; HRMS (ESI) $[M + H]^+$ calcd. for $C_{20}H_{14}FNO_4$: 352.0975; found: 352.0982.

(15, $C_{21}H_{17}NO_5$). White sold; Yield 68%; m.p. 150–152 °C; ^{1}H NMR (500 MHz, Chloroform-*d*) δ 8.15 (s, 1H), 7.83 (d, J = 16.0 Hz, 1H), 7.59–7.53 (m, 4H), 7.37–7.30 (m, 2H), 6.94–6.92 (m, 2H), 6.45 (d, J = 16.0 Hz, 1H), 3.85 (s, 3H), 2.48 (s, 3H); ^{13}C NMR (126 MHz, $CDCl_3$) δ 164.70, 161.83, 159.30, 154.32, 146.52, 143.34, 132.92, 130.12, 129.05, 126.91, 124.94, 123.67, 118.57, 116.67, 114.44, 112.54, 77.32, 77.27, 77.07, 76.81, 55.46, 15.91; HRMS (ESI) $[M + H]^+$ calcd. for $C_{21}H_{17}NO_5$: 364.1178; found: 364.1182.

(16, $C_{20}H_{14}N_2O_6$). Yellow sold; Yield 70%; m.p. 221–222 °C; ^{1}H NMR (500 MHz, Chloroform-*d*) δ 8.30 – 8.27 (m, 2H), 8.16 (s, 1H), 7.91 (d, J = 16.0 Hz, 1H), 7.76–7.74 (m, 2H), 7.60 (ddd, J = 14.2, 8.0, 1.6 Hz, 2H), 7.39–7.31 (m, 2H), 6.73 (d, J = 16.1 Hz, 1H), 2.50 (s, 3H); ^{13}C NMR (126 MHz, $CDCl_3$) δ 163.40, 162.80, 159.19, 154.37, 148.78, 143.74, 143.51, 140.12, 133.13, 129.09, 128.95, 125.02, 124.29, 123.35, 119.71, 118.46, 116.75, 77.30, 77.25, 77.05, 76.79, 16.02; HRMS (ESI) $[M + H]^+$ calcd. for $C_{20}H_{14}N_2O_6$: 379.0923; found: 379.0927.

(17, $C_{21}H_{14}F_3NO_4$). White sold; Yield 75%; m.p. 169–171 °C; ^{1}H NMR (500 MHz, Chloroform-*d*) δ 8.15 (s, 1H), 7.88 (d, J = 16.1 Hz, 1H), 7.71–7.65 (m, 4H), 7.61–7.56 (m, 2H), 7.37–7.30 (m, 2H), 6.66 (d, J = 16.1 Hz, 1H), 2.49 (s, 3H); ^{13}C NMR (126 MHz, $CDCl_3$) δ 163.76, 162.54, 159.21, 154.35, 144.86, 143.46, 133.06, 129.07, 128.47, 126.00, 125.97, 124.99, 123.42, 118.49, 117.96, 116.70, 77.32, 77.07, 76.81, 15.97; HRMS (ESI) $[M + H]^+$ calcd. for $C_{21}H_{14}F_3NO_4$: 402.0944; found: 402.0951.

(18, $C_{20}H_{15}NO_5$). White sold; Yield 75%; m.p. 156–158 °C; ^{1}H NMR (500 MHz, DMSO d_6) δ 10.12 (d, J = 23.3 Hz, 1H), 8.33 (d, J = 23.1 Hz, 1H), 7.93 (d, J = 8.4 Hz, 1H), 7.78–7.48 (m, 5H), 6.83 (d, J = 8.5 Hz, 2H), 6.61 (d, J = 16.0 Hz, 1H), 2.37 (s, 4H); ^{13}C NMR (126 MHz, DMSO) δ 164.49, 162.21, 160.73, 159.15, 154.18, 146.98, 143.66, 133.60, 131.22, 130.00, 125.51, 125.44, 123.73, 118.89, 116.68, 116.30, 116.26, 111.91, 40.56, 40.47, 40.39, 40.30, 40.22, 40.13, 40.06, 39.97, 39.89, 39.80, 39.63, 39.46, 16.12; HRMS (ESI) $[M + H]^+$ calcd. for $C_{20}H_{15}NO_5$: 350.1018; found: 350.1025.

(19, $C_{20}H_{13}ClBrNO_4$). White sold; Yield 70%; m.p. 201–203 °C; ^{1}H NMR (500 MHz, Chloroform-*d*) δ 8.12 (s, 1H),

7.81 (d, J = 16.0 Hz, 1H), 7.57–7.53 (m, 2H), 7.51 (d, J = 8.3 Hz, 1H), 7.47–7.43 (m, 2H), 7.37 (d, J = 1.9 Hz, 1H), 7.30 (dd, J = 8.4, 2.0 Hz, 1H), 6.57 (d, J = 16.0 Hz, 1H), 2.47 (s, 3H); ^{13}C NMR (126 MHz, $CDCl_3$) δ 164.00, 161.98, 158.54, 154.54, 145.53, 142.56, 139.10, 133.00, 132.30, 129.81, 129.70, 125.68, 125.24, 123.42, 117.09, 117.08, 115.88, 77.31, 77.26, 77.05, 76.80, 15.87; HRMS (ESI) $[M + H]^+$ calcd. for $C_{20}H_{13}ClBrNO_4$: 483.9343; found: 483.9348.

(20, $C_{20}H_{13}Br_2NO_4$). White sold; Yield 70%; m.p. 190–191 °C; ^{1}H NMR (500 MHz, Chloroform-*d*) δ 8.11 (s, 1H), 7.81 (d, J = 16.0 Hz, 1H), 7.58–7.53 (m, 3H), 7.48–7.42 (m, 4H), 6.57 (d, J = 16.0 Hz, 1H), 2.47 (s, 3H); ^{13}C NMR (126 MHz, $CDCl_3$) δ 164.00, 162.00, 158.48, 154.44, 145.56, 142.65, 132.99, 132.31, 129.89, 129.71, 128.52, 127.21, 125.25, 123.68, 120.05, 117.43, 115.86, 77.30, 77.25, 77.05, 76.80, 15.88; HRMS (ESI) $[M + H]^+$ calcd. for $C_{20}H_{13}Br_2NO_4$: 489.9282; found: 489.9286.

(21, $C_{20}H_{13}BrFNO_4$). White sold; Yield 70%; m.p. 186–188 °C; ^{1}H NMR (500 MHz, Chloroform-*d*) δ 8.13 (s, 1H), 7.81 (d, J = 16.0 Hz, 1H), 7.56 (dd, J = 7.0, 5.0 Hz, 3H), 7.46 (d, J = 8.2 Hz, 2H), 7.08 (dt, J = 8.3, 1.7 Hz, 2H), 6.57 (d, J = 16.0 Hz, 1H), 2.47 (s, 3H); ^{13}C NMR (126 MHz, $CDCl_3$) δ 166.22, 164.18, 164.03, 162.06, 158.79, 155.63, 155.53, 145.49, 142.81, 133.01, 132.30, 132.20, 130.81, 130.73, 129.70, 125.23, 122.31, 122.28, 115.91, 115.27, 115.24, 113.45, 113.27, 104.53, 104.32, 77.30, 77.05, 76.79, 15.89; HRMS (ESI) $[M + H]^+$ calcd. for $C_{20}H_{13}BrFNO_4$: 430.0085; found: 430.0085.

(22, $C_{21}H_{16}BrNO_4$). White sold; Yield 70%; m.p. 198–201 °C; ^{1}H NMR (500 MHz, Chloroform-*d*) δ 8.14 (s, 1H), 7.83 (d, J = 16.0 Hz, 1H), 7.59–7.55 (m, 2H), 7.48–7.45 (m, 3H), 7.20–7.13 (m, 2H), 6.60 (d, J = 16.0 Hz, 1H), 2.50 (s, 6H); ^{13}C NMR (126 MHz, $CDCl_3$) δ 164.11, 162.51, 159.51, 154.52, 145.32, 144.68, 143.46, 133.06, 132.28, 129.69, 128.74, 126.25, 125.15, 122.21, 116.84, 116.16, 116.06, 77.30, 77.25, 77.05, 76.80, 22.03, 15.97; HRMS (ESI) $[M + H]^+$ calcd. for $C_{21}H_{16}BrNO_4$: 426.0336; found: 426.0335.

(23, $C_{21}H_{16}BrNO_5$). White sold; Yield 70%; m.p. 205–210 °C; ^{1}H NMR (500 MHz, Chloroform-*d*) δ 8.11 (s, 1H), 7.80 (d, J = 16.0 Hz, 1H), 7.57–7.53 (m, 2H), 7.49–7.43 (m, 3H), 6.88 (dd, J = 8.6, 2.4 Hz, 1H), 6.83 (d, J = 2.4 Hz, 1H), 6.57 (d, J = 16.0 Hz, 1H), 3.90 (s, 3H), 2.47 (s, 3H); ^{13}C NMR (126 MHz, $CDCl_3$) δ 164.16, 163.91, 162.61, 159.61, 156.44, 145.25, 143.58, 133.08, 132.27, 130.14, 129.68, 125.13, 119.67, 116.12, 113.44, 112.20, 100.53, 77.30, 77.25, 77.05, 76.79, 55.93, 15.93; HRMS (ESI) $[M + H]^+$ calcd. for $C_{21}H_{16}BrNO_5$: 442.0251; found: 442.0285.

(24, $C_{20}H_{13}ClBrNO_4$). White sold; Yield 70%; m.p. 201–203 °C; ^{1}H NMR (500 MHz, Chloroform-*d*) δ 8.06 (s, 1H), 7.82 (d, J = 16.0 Hz, 1H), 7.58–7.53 (m, 5H), 7.46 (d, J = 8.2 Hz, 2H), 7.33–7.30 (m, 1H), 6.58 (d, J = 16.0 Hz, 1H), 2.47 (s, 3H); ^{13}C NMR (126 MHz, $CDCl_3$) δ 163.98, 161.87, 158.62, 152.67, 145.61, 142.03, 132.99, 132.94, 132.31, 130.28, 129.72, 128.06, 125.26, 124.73, 119.52, 118.18, 115.82, 77.30, 77.25, 77.05, 76.79, 15.92; HRMS (ESI) $[M + H]^+$ calcd. for $C_{20}H_{13}ClBrNO_4$: 447.9771; found: 447.9769.

(25, $C_{20}H_{13}Br_2NO_4$). White sold; Yield 65%; m.p. 171–172 °C; ^{1}H NMR (500 MHz, Chloroform-*d*) δ 8.08 (s, 1H), 7.61–7.57 (m, 3H), 7.55–7.51 (m, 3H), 7.49–7.47 (m, 2H), 6.60 (d, J = 16.0 Hz, 1H), 2.50 (s, 3H); ^{13}C NMR (126 MHz, $CDCl_3$) δ 164.00, 161.85, 158.57, 153.14, 145.62, 141.94, 135.74, 132.99, 132.31, 131.13, 129.72, 125.26, 124.69, 120.01, 118.45, 117.55, 115.82, 77.30, 77.25, 77.04, 76.86, 76.79, 15.92; HRMS (ESI) $[M + H]^+$ calcd. for $C_{20}H_{13}Br_2NO_4$: 489.9282; found: 489.9284.

(26, $C_{20}H_{13}BrFNO_4$). White sold; Yield 65%; m.p. 192–193 °C; ^{1}H NMR (500 MHz, Chloroform-*d*) δ 8.08 (s, 1H), 7.81 (d, J = 15.9 Hz, 1H), 7.55 (d, J = 8.3 Hz, 2H), 7.45 (d, J = 8.3 Hz, 2H), 7.37–7.29 (m, 2H), 7.24 (d, J = 2.9 Hz, 1H), 6.57 (d, J = 16.0 Hz, 1H), 2.47 (s, 3H); ^{13}C NMR (126 MHz, $CDCl_3$) δ 163.98, 161.95, 159.87, 158.83, 157.92, 150.50, 150.48, 145.57, 142.32, 142.30, 132.99, 132.30, 129.71, 125.25, 124.70, 120.64, 120.44, 119.23, 119.16, 118.38, 118.32, 115.84, 114.19, 114.00, 77.31, 77.26, 77.05, 76.80, 15.91; HRMS (ESI) $[M + H]^+$ calcd. for $C_{20}H_{13}BrFNO_4$: 430.0089; found: 430.0085.

(27, $C_{21}H_{16}BrNO_4$). White sold; Yield 70%; m.p. 182–183 °C; ^{1}H NMR (500 MHz, Chloroform-*d*) δ 8.09 (s, 1H), 7.85–7.78 (m, 1H), 7.58–7.53 (m, 2H), 7.48–7.43 (m, 2H), 7.39 (dd, J = 8.4, 2.1 Hz, 1H), 7.34 (d, J = 2.1 Hz, 1H), 7.25–7.21 (m, 1H), 6.58 (d, J = 16.0 Hz, 1H), 2.47 (s, 3H), 2.42 (s, 3H); ^{13}C NMR (126 MHz, $CDCl_3$) δ 164.12, 162.47, 159.48, 152.52, 145.39, 143.43, 134.76, 134.14, 133.05, 132.29, 129.70, 128.70, 125.17, 123.33, 118.27, 116.41, 116.01, 77.30, 77.25, 77.05, 76.79, 20.82, 15.99; HRMS (ESI) $[M + H]^+$ calcd. for $C_{21}H_{16}BrNO_4$: 426.0342; found: 426.0335.

(28, $C_{21}H_{16}BrNO_5$). White sold; Yield 70%; m.p. 251–253 °C; ^{1}H NMR (500 MHz, Chloroform-*d*) δ 8.11 (s, 1H), 7.81 (d, J = 16.0 Hz, 1H), 7.56 (d, J = 8.2 Hz, 2H), 7.46 (d, J = 8.2 Hz, 2H), 7.29 (d, J = 9.1 Hz, 1H), 7.17 (dd, J = 9.1, 2.9 Hz, 1H), 6.98 (d, J = 2.9 Hz, 1H), 6.58 (d, J = 16.0 Hz, 1H), 3.85 (s, 3H), 2.48 (s, 3H); ^{13}C NMR (126 MHz, $CDCl_3$) δ 164.10, 162.40, 159.41, 156.36, 148.87, 145.42, 143.26, 133.03, 132.29, 132.27, 129.70, 125.19, 123.72, 121.08, 118.86, 117.75, 115.99, 110.54, 77.30, 77.25, 77.05, 76.80, 55.89, 15.95; HRMS (ESI) $[M + H]^+$ calcd. for $C_{21}H_{16}BrNO_5$: 442.0251; found: 442.0285.

4.3. a-Glucosidase inhibition and kinetics assay

The α-glucosidase inhibitory activity of coumarin derivatives **1**–**28** was assayed using PNPG as substrate (Taha et al., 2018; Carreiro et al., 2014). The α-glucosidase (0.1 U/mL) and test compound was added into phosphate buffer saline (0.1 M, pH 6.8), followed by an incubation for 10 min at 37 °C. After PNPG (0.1 U/mL) was added, the absorbance change was measured at 405 nm. The test compound was dissolved in DMSO, and acarbose was used as a positive control. All experiments were performed 4 times.

The enzyme inhibitory kinetics (Deng et al., 2022) of compound **20** were obtained by the plots of enzymatic reaction rate vs enzyme concentration with or without compound **20**, and the substrate inhibitory kinetics (Hu et al., 2021) were measured using the Lineweaver-Burk plot of enzymatic reaction rate vs substrate concentration with or compound **20**.

4.4. 3D fluorescence spectra assay

Compound **20** (2 μM) was added into α-glucosidase (5 μM) and incubated for 5 min. Then the 3D fluorescence spectra of the mixture were recorded (Zeng et al., 2016). The excitation and emission wavelengths were 200–600 nm. The slit width is 2.5 nm. The data was imported into Matlab for processing.

4.5. CD spectroscopy

Compound **20** (35 μM) was added into α-glucosidase (31 μM) and incubated for 5 min. Then the CD spectrum of the mixture was recorded (Peng et al., 2015). The CDNN was used to analyze the proportion of secondary conformation of protein.

4.6. Molecular docking

SYBYL software was used to simulate the interaction between compound **20** and α-glucosidase (Yu et al., 2018). The homology model of α-glucosidase was constructed according to previous works (Wang et al., 2017; Wang et al., 2018) and optimized by procedure of removing water molecules, adding hydrogen atoms, adding charge, and repairing end residues, followed by the generation of active pocket. Compound **20** was charged with Gasteiger-Hückle and prepared by energy minimization program. Thus, the docking between compounds and target protein was operated in the default format, and the results were visualized by Pymol and Discover studio software.

Declaration of Competing Interest

The authors declare that they have no known competing financial interests or personal relationships that could have appeared to influence the work reported in this paper.

Acknowledgements

This work was financially supported by the Fundamental and Applied Basic Research Fund of Guangdong Province (No. 2022A1515011657), Department of Education of Guangdong Province (Nos. 2019KZDXM035, 2021KTSCX135, 2021KCXTD044), and Jiangmen Science and Technology Plan Project (2021030103150006664).

Appendix A. Supplementary material

Supplementary data to this article can be found online at https://doi.org/10.1016/j.arabjc.2022.104072.

References

Ali, F., Khan, K.M., Salar, U., Taha, M., Ismail, N.H., Wadood, A., Riaz, M., Perveen, S., 2017. Hydrazinyl arylthiazole based pyridine scaffolds: Synthesis, structural characterization, in vitro α-glucosidase inhibitory activity, and in silico studies. Eur. J. Med. Chem. 138, 255–272.

Carreiro, E.P., Louro, P., Adriano, G., Guedes, R.A., Vannuchi, N., Costa, A.R., Antunes, C.M.M., Guedes, R.C., Burke, A.J., 2014. 3-Hydroxypyrrolidine and (3, 4)-dihydroxypyrrolidine derivatives: Inhibition of rat intestinal α-glucosidase. Bioorg. Chem. 54, 81–88.

Deng, X.Y., Ke, J.J., Zheng, Y.Y., Li, D.L., Zhang, K., Zheng, X., Wu, J.Y., Xiong, Z., Wu, P.P., Xu, X.T., 2022. Synthesis and bioactivities evaluation of oleanolic acid oxime ester derivatives as alpha-glucosidase and alpha-amylase inhibitors. J. Enzyme. Inhib. Med. Chem. 37, 451–461.

Hameed, S., Kanwal, F., Seraj, R., Rafique, S., Chigurupati, A., Wadood, A.U., Rehman, V., Venugopal, U., Salar, M., Taha, K. M.K., 2019. Synthesis of benzotriazoles derivatives and their dual potential as alpha-amylase and alpha-glucosidase inhibitors *in vitro*: Structure-activity relationship, molecular docking, and kinetic studies. Eur. J. Med. Chem. 183, 111677.

Hedrington, M.S., Davis, S.N., 2019. Considerations when using alpha-glucosidase inhibitors in the treatment of type 2 diabetes. Expert. Opin. Pharmaco. 20, 2229–2235.

Hosseini Ghazvini, S.M.B., Safari, P., Mobinikhaledi, A., Moghanian, H., Rasouli, H., 2018. Synthesis, characterization, anti-diabetic potential and DFT studies of 7-hydroxy-4-methyl-2-oxo-2H-chromene-8-carbaldehyde oxime. Spectrochim. Acta A. 205, 111–131.

Hu, C.M., Wang, W.J., Ye, Y.N., Kang, Y., Lin, J., Wu, P.P., Li, D. L., Bai, L.P., Xu, X.T., Li, B.Q., Zhang, K., 2021. Novel cinnamic acid magnolol derivatives as potent alpha-glucosidase and alpha-amylase inhibitors: Synthesis, in vitro and in silico studies. Bioorg. Chem. 116, 105291.

Imran, S., Taha, M., Ismail, N.H., Kashif, S.M., Rahim, F., Jamil, W., Hariono, M., Yusuf, M., Wahab, H., 2015. Synthesis of novel flavone hydrazones: *In-vitro* evaluation of α-glucosidase inhibition, QSAR analysis and docking studies. Eur. J. Med. Chem. 105, 156–170.

Kassa, J., Misik, J., Hatlapatkova, J., Zdarova Karasova, J., Sepsova, V., Caisberger, F., Pejchal, J., 2017. The evaluation of the reactivating and neuroprotective efficacy of two newly prepared bispyridinium oximes (K305, K307) in Tabun-poisoned rats-a comparison with trimedoxime and the oxime K203. Molecules 22, 1152.

Matos, M.J., Vazquez-Rodriguez, S., Fonseca, A., Uriarte, E., Santana, L., Borges, F., 2017. Heterocyclic antioxidants in nature: Coumarins. Curr. Org. Chem. 21, 311–324.

Peng, X., Zhang, G.W., Liao, Y.J., Gong, D.M., 2015. Inhibitory kinetics and mechanism of kaempferol on alpha-glucosidase. Food Chem. 190, 207–215.

Proença, C., Freitas, M., Ribeiro, D., Oliveira, E.F., Sousa, J.L., Tomé, S.M., Fernandes, E., 2017. α-Glucosidase inhibition by flavonoids: An *in vitro* and *in silico* structure-activity relationship study. J. Enzyme. Inhib. Med. Ch. 32, 1216–1228.

Rasouli, H., Hosseini-Ghazvini, S.M., Adibi, H., Khodarahmi, R., 2017. Differential alpha-amylase/alpha-glucosidase inhibitory activities of plant-derived phenolic compounds: A virtual screening perspective for the treatment of obesity and diabetes. Food Funct. 8, 1942–1954.

Sahni, T., Sharma, S., Verma, D., Kaur, P., 2021. Overview of coumarins and its derivatives: Synthesis and biological activity. Lett. Org. Chem. 18, 880–902.

Salar, U., Taha, M., Khan, K.M., Ismail, N.H., Imran, S., Perveen, S., Gul, S., Wadood, A., 2016. Syntheses of new 3-thiazolyl coumarin derivatives, *in vitro* alpha-glucosidase inhibitory activity, and molecular modeling studies. Eur. J. Med. Chem. 122, 196–204.

Santos, C.M.M., Freitas, M., Fernandes, E., 2018. A comprehensive review on xanthone derivatives as alpha-glucosidase inhibitors. Eur. J. Med. Chem. 157, 1460–1479.

Schepetkin, I.A., Plotnikov, M.B., Khlebnikov, A.I., Plotnikova, T. M., Quinn, M.T., 2021. Oximes: Novel therapeutics with anticancer and anti-inflammatory potential. Biomolecules 11, 777.

Sohretoglu, D., Sari, S., Barut, B., Ozel, A., 2018. Discovery of potent alpha-glucosidase inhibitor flavonols: Insights into mechanism of action through inhibition kinetics and docking simulations. Bioorg. Chem. 79, 257–264.

Song, Y.H., Kim, D.W., Curtis-Long, M.J., Park, C., Son, M., Kim, J. Y., Yuk, H.J., Lee, K.W., Park, K.H., 2016. Cinnamic acid amides from Tribulus terrestris displaying uncompetitive alpha-glucosidase inhibition. Eur. J. Med. Chem. 114, 201–208.

Stefanachi, A., Leonetti, F., Pisani, L., Catto, M., Carotti, A., 2018. Coumarin: A natural, privileged and versatile scaffold for bioactive compounds. Molecules 23, 250.

Taha, M., Shah, S.A.A., Afifi, M., Imran, S., Sultan, S., Rahim, F., Khan, K.M., 2018. Synthesis, α-glucosidase inhibition and molec-

ular docking study of coumarin based derivatives. Bioorg. Chem. 77, 586–592.

Taha, M., Shah, S.A.A., Afifi, M., Imran, S., Sultan, S., Rahim, F., Khan, K.M., 2018. Synthesis, α-glucosidase inhibition and molecular docking of coumarin based derivatives. Bioorg. Chem. 77, 586–592.

Tran, T.M., Nguyen, V.K., Duong, T.H., Tran, T.N., Nguyen, N.H., Devi, A.P., Chavasiri, W., Dinh, M.H., Tran, N.M., Sichaem, J., 2022. Maydisone, a novel oxime polyketide from the cultures of Bipolaris maydis. Nat. Prod. Res. 36, 102–107.

Tsoutsouki, J., Wunna, W., Chowdhury, A., Chowdhury, T.A., 2020. Advances in the management of diabetes: therapies for type 2 diabetes. Postgrad. Med. J. 96, 610–618.

Wang, G., He, D., Li, X., Li, J., Peng, Z., 2016. Design, synthesis and biological evaluation of novel coumarin thiazole derivatives as α-glucosidase inhibitors. Bioorg. Chem. 65, 167–174.

Wang, G.C., Wang, J., Xie, Z.Z., Chen, M., Li, L.Y., Peng, Y.P., Chen, S., Li, W.B., Deng, B., 2017. Discovery of 3,3-di(indolyl) indolin-2-one as a novel scaffold for α-glucosidase inhibitors: *In silico* studies and SAR predictions. Bioorg. Chem. 72, 228–233.

Wang, G.C., Peng, Z.Y., Gong, Z.P., Li, Y.J., 2018. Synthesis, biological evaluation, and docking studies of novel 5,6-diaryl-1,2,4-triazine thiazole derivatives as a new class of α-glucosidase inhibitors. Bioorg. Chem. 78, 195–200.

Wu, Y., Xu, J., Liu, Y., Zeng, Y., Wu, G., 2020. A review on anti-tumor mechanisms of coumarins. Front. Oncol. 10, 592853.

Xu, X.T., Deng, X.Y., Chen, J., Liang, Q.M., Zhang, K., Li, D.L., Wu, P.P., Zheng, X., Zhou, R.P., Jiang, Z.Y., Ma, A.J., Chen, W. H., Wang, S.H., 2020. Synthesis and biological evaluation of coumarin derivatives as alpha-glucosidase inhibitors. Eur. J. Med. Chem. 189, 112013.

Yu, Q., Wang, F., Hu, X., Xing, G., Deng, R., Guo, J., Cheng, A., Wang, J., Hao, J., Zhao, D., Teng, M., Zhang, G., 2018. Comparison of two docking methods for peptide-protein interactions. J. Sci. Food. Agric. 98, 3722–3727.

Zeng, L., Zhang, G.W., Lin, S.Y., 2016. Inhibitory Mechanism of apigenin on alpha-glucosidase and synergy analysis of flavonoids. J. Arg Food Chem. 64, 6939–6949.